Charge-Tuned CO Activation over a χ-Fe_5C_2 Fischer–Tropsch Catalyst

Bingxu Chen,[†,⊥] Di Wang,[†,⊥] Xuezhi Duan,[*,†] Wei Liu,[‡] Yefei Li,[§] Gang Qian,[†] Weikang Yuan,[†] Anders Holmen,[∥] Xinggui Zhou,[†] and De Chen[*,∥]

[†]State Key Laboratory of Chemical Engineering, East China University of Science and Technology, 130 Meilong Road, Shanghai 200237, China

[‡]Nano Structural Materials Center, Nanjing University of Science and Technology, Nanjing 210094, China

[§]Collaborative Innovation Center of Chemistry for Energy Material, Fudan University, Shanghai 200433, China

[∥]Department of Chemical Engineering, Norwegian University of Science and Technology, Trondheim 7491, Norway

Supporting Information

ABSTRACT: We performed DFT calculations to understand CO activation over a χ-Fe_5C_2 Fischer–Tropsch catalyst. The χ-Fe_5C_2 catalyst exhibits unique CO activation behaviors, and the BEP relation is nearly valid for this system. The physical basis of this relation mainly originates from the site-dependent charge of the involved surface Fe atoms for the CO activation. This descriptor is also applicable to describe the CO activation on the χ-Fe_5C_2 catalyst with more complex surface properties involving K promoter, nonstoichiometric termination, and/or carbon vacancy. The insights revealed here might guide the rational catalyst design via surface electronic modification.

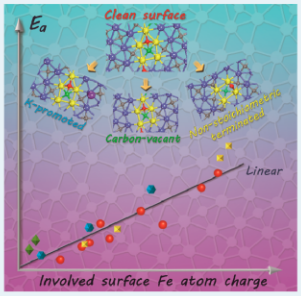

KEYWORDS: *χ-Fe_5C_2 Fischer–Tropsch synthesis, CO activation, structure–activity relationship, density functional theory, charge density analysis*

Iron-catalyzed Fischer–Tropsch synthesis (FTS) is of burgeoning interest in enabling direct conversion of CO-rich syngas derived from coal and biomass into clean fuels and lower olefins.[1−8] It is recognized as a structure-sensitive reaction,[9,10] meaning a dependence of the FTS activity on the particle size of the active phase. Recently, Hägg iron carbide, χ-Fe_5C_2, has been suggested as dominant active phase for the FTS.[11−22] A central prerequisite for the knowledge-based design of the χ-Fe_5C_2 catalyst is to understand the nature of the active sites. However, it remains a substantial challenge to reveal the origin of the size effects on the FTS activity, which is complicated by complex/dynamic catalyst surface properties and crystal phase composition (e.g., iron, iron oxides, and iron carbides) under the realistic reaction conditions.[5,6,11,12,19−21]

CO activation, a key step in the initiation of the FTS, is usually employed as a probe reaction to understand the difference in the FTS activities of different catalysts/surfaces.[23−26] The reaction energy and d-band center have been theoretically suggested as the suitable descriptors of the CO activation reactivity.[27−31] However, these analyses have been limited to the trends within various transition metal catalysts with the similar surface geometries. To the best of our knowledge, it remains an open question whether these two descriptors can be applicable or other ones can be discriminated to describe the CO activation on different crystal facets over the given χ-Fe_5C_2 catalyst.

Previous studies showed that the χ-Fe_5C_2 catalyst compared to the monometallic FTS catalysts (e.g., Ru and Co)[32,33] exhibits unique exposed crystal facet composition, mainly consisting of high Miller-index facets such as (510) and (021).[34] Unexpectedly, the thermodynamically stable terrace-like χ-Fe_5C_2(510) surface is more active than the step-like surfaces (i.e., χ-Fe_5C_2(010), (001), and (100)).[18,34−37] This indicates significantly different CO activation behaviors. In addition to the stoichiometrically terminated clean χ-Fe_5C_2 surface, the presence of the nonstoichiometric termination,[38] B_5 site,[18,33] carbon vacancy,[37,39,40] and promoter[14,41,42] (Figure 1) also affects CO activation. An attempt is therefore necessary to fully explore the CO activation on different χ-Fe_5C_2 catalyst surfaces, aiming to unravel the nature of the active sites and then guide the rational design of the catalyst.

To address these unresolved mechanistic details of the CO activation over the given χ-Fe_5C_2 FTS catalyst, we resorted here to extensive spin-polarized density functional theory (DFT) calculations (more computational details shown in Supporting Information (SI), Table S1). The unique CO activation behaviors and Brønsted–Evans–Polanyi (BEP) relation were unambiguously investigated and rationalized. The physical basis of this relation mainly originated from the difference in the

Received: December 19, 2017
Revised: January 26, 2018
Published: February 21, 2018

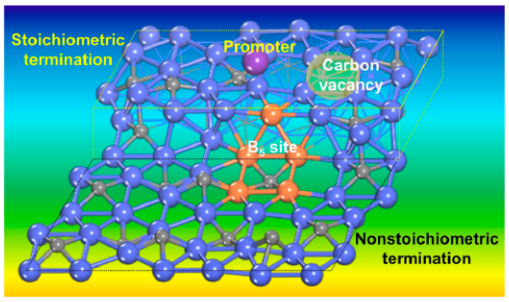

Figure 1. Illustration of the geometric structure of typical χ-Fe_5C_2 surface (Fe atoms in blue and C atoms in gray) involving (non)stoichiometric termination, B_5 site (orange), carbon vacancy (yellow), and promoter (purple).

electronic properties in terms of the spatially resolved atomic charge of the involved surface Fe atoms for the CO activation rather than the work function and d-band center. This descriptor was also applicable to describe the CO activation on the χ-Fe_5C_2 catalyst with more complex surface properties involving K promoter, nonstoichiometric termination, and/or carbon vacancy.

We started with systematic investigations of CO activation with and without H-assisted (Figure 2a) on six representative χ-

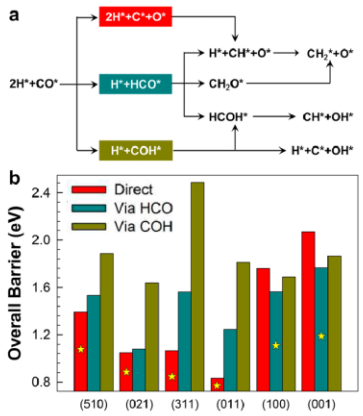

Figure 2. (a) Schematic of three kinds of CO activation mechanisms, i.e., direct CO dissociation, H-assisted CO dissociation via HCO intermediate, and H-assisted CO dissociation via COH intermediate, where the empty site (*) is not presented in the elementary steps for the sake of clarity. (b) Calculated overall barriers of three preferred CO activation pathways for the three CO activation mechanisms on the χ-Fe_5C_2(510), (021), (311), (011), (100), and (001) surfaces, in which the preferred CO activation pathways are marked with yellow stars for each surface.

Fe_5C_2 surfaces with stoichiometric terminations, i.e., two thermodynamically stable terrace-like (510) and (021) surfaces,[34] three step-like (311), (011), and (100) surfaces with B_5-like sites,[18,33,41] and one step-like (001) surface without B_5-like site[36] (Figure S1). All the identified stable CO adsorption configurations, most stable adsorbed intermediates adsorption, and transition states configurations as well as the associated structural parameters, adsorption energies, and activation barriers are listed in SI Tables S2−S3 and Figures S2−S5. It is unexpected that there is no direct relationship of the structural parameters with the CO adsorption energy as well as the CO activation barrier. However, it is clearly seen in Figure 2b that for the preferred CO activation pathway, the former four surfaces prefer the direct CO dissociation, while the last two surfaces prefer the H-assisted CO dissociation. More interestingly, the preferred direct CO dissociation pathways over the former four surfaces correspond to lower overall barriers than the preferred H-assisted CO dissociation pathways over the last two surfaces (Figure 2b). Similar phenomena are also observed on the CO activation over Co catalyst,[32] i.e., the direct CO dissociation corresponding to lower barrier and thus higher FTS activity. On the basis of these analyses, the direct CO dissociation can be used as the model reaction to fundamentally understand the CO activation on the χ-Fe_5C_2 catalyst and then unravel the nature of the active sites.

Previous studies demonstrated that monometallic FTS catalyst surfaces with B_5 sites show significant weakening of the C−O bonds for the CO dissociation precursor state and thus low CO activation barriers.[43−45] However, our cases, i.e., CO adsorption and activation on the χ-Fe_5C_2 surfaces with the B_5-like sites, do not follow similar trends. Specifically, the (011) surface exhibits the lowest CO activation barrier, but its C−O bond elongation is not significant compared to those on the terrace-like (510) and (021) surfaces and the step-like (100) surface. These results indicate remarkably different CO activation behaviors on the χ-Fe_5C_2 catalyst compared to the monometallic FTS catalysts,[43−46] calling for an in-depth understanding.

In contrast to the monometallic FTS catalysts, the χ-Fe_5C_2 catalyst, classified as the trigonal prismatic carbide, exhibits a weak surface symmetry due to the existence of the interstitial carbon atoms between the close-packed iron atoms.[6,11,47] This leads to different local environments of the iron atoms to activate CO on different crystal facets (Figure S6) and thus a large complexity in the fundamental understanding of the CO activation. The solution to reduce the complexity is to develop a suitable reactivity descriptor from the generality of the scaling relations.[48,49]

The most successful example of the scaling relations is the well-known Brønsted−Evans−Polanyi (BEP) relation,[50−52] predicting the activation barrier from the reaction energy (ΔE_r). Along this line, we studied direct dissociation of CO on nine typical χ-Fe_5C_2 surfaces and then plotted the forward activation barrier ($E_{a,forward}$) with the ΔE_r. Apparently, there is a nearly linear relation (Figure 3a), suggesting that the reaction energy could be a descriptor for the CO activation on different χ-Fe_5C_2 catalyst surfaces.

To explain and rationalize the above BEP relation, we employed Hammond's postulate[53,54] and compared the stability of the transition states. It is shown that the energy of the transition states is close to neither the reactant nor the product (SI Figure S7). We further plotted the reverse activation barrier ($E_{a,reverse}$) with the ΔE_r and found that the corresponding linear relation is slightly worse for the reverse reaction as opposed to the forward reaction (Figure 3b), indicating that the TSs are "late" along the reaction coordinate.[53,54] Additionally, the C−O bond length at the TSs is much longer than that in the adsorbed CO (Figure 3c), suggesting that the TSs of the CO activation on the χ-Fe_5C_2 catalyst is structurally more product-like than reactant-like.[53,54] Therefore, it is rationally deduced that the BEP relation mainly relates to the stability of the product. This is further evidenced by a slightly better linear

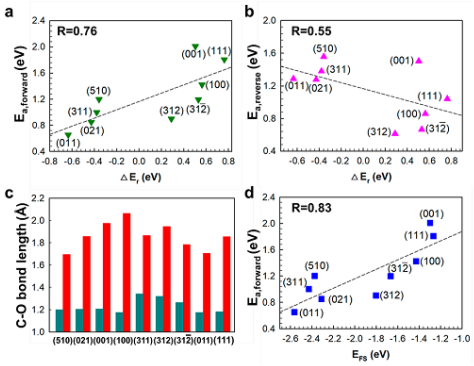

Figure 3. Plots of (a) the forward barrier ($E_{a,forward}$) and (b) the reverse barrier ($E_{a,reverse}$) for CO activation against the corresponding reaction energy (ΔE_r) on the nine typical χ-Fe_5C_2 surfaces. (c) C−O bond lengths of the favorably adsorbed CO (cyan) and the TSs (red). (d) Plots of the forward barrier against the stability of the final states (E_{FS}). Linear fits and regression coefficients (R) are given in each case.

relation between the $E_{a,forward}$ and the energy of the final states (Figure 3d).

To understand the physical basis of the above linear relations, the electronic structures of the nine χ-Fe_5C_2 surfaces, in principle determining completely the catalytic properties,[27] were analyzed in depth. First, we investigated the possible trends in the work functions of the different χ-Fe_5C_2 surfaces. However, there is a very poor linear relation between the CO activation barrier and the work function (SI Figure S8a). This is most likely because the work function is an average over the whole catalyst surface and thus an inadequate descriptor to describe the effects of the local environment of the iron atoms over the different χ-Fe_5C_2 surfaces, which is a local site property. Subsequently, we plotted the d-band center of the involved surface Fe atoms for the CO activation with the CO activation barrier (SI Figure S8b). However, the d-band model[55,56] does not give a good description of the CO activation barrier for the different χ-Fe_5C_2 surfaces. This could be explained by the fact that unless the set of metals with the similar surface environments being screened is restricted, there would exist a linear relation between the d-band center and the activation barrier.[31,57,58]

Taking into account that the χ-Fe_5C_2 catalyst consists of positively charged Fe atoms and negatively charged C atoms, the typical χ-Fe_5C_2(510) surface was taken as an example to understand the CO activation by analyzing charge density difference of the TS. As shown in Figure 4a, the Fe atoms show decreased electron density (light-blue map), while the surface C in the (I) region, the TS in the (II) region, and the subsurface C in the (III) region exhibit increased electron density (yellow map). This indicates a competition of electron withdrawing capacity from the Fe atoms between the TS and the (sub)surface carbon of the χ-Fe_5C_2 catalyst. In this context, one could expect that the nine χ-Fe_5C_2 surfaces exhibit different competition due to the different local environment of the involved surface Fe atoms.

Different from the analyses of the work function and d-band center, the charge density analysis based on the partition of the total charge density is an effective method to quantify the spatially resolved atomic charge of the iron carbides surfaces.[35,59] Here, we employed two popular methods, i.e.,

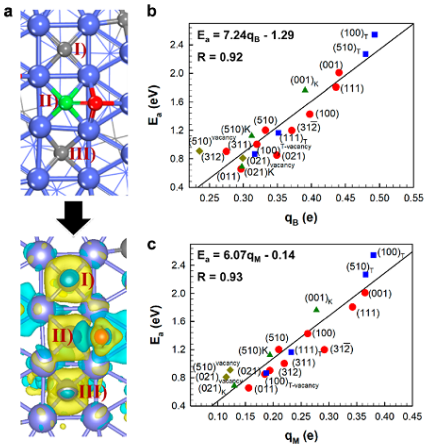

Figure 4. (a) Configuration and the corresponding charge density difference of the TS for CO activation on χ-Fe_5C_2(510) surface, where (I), (II), and (III) regions represent the surface C, the TS, and the subsurface C, respectively. Yellow and light-blue isosurfaces represent accumulation and depletion of electronic density. Trends in the direct CO dissociation barrier (E_a) as a function of the average Bader charge (q_B) (b) and the average Mulliken charge (q_M) (c) of the involved surface Fe atoms for the CO activation. The ▲, ■, and ◆ represent the cases involving K promoter, nonstoichiometric termination, and carbon vacancy, respectively. Linear fits and the related regression equations and coefficients (R) are given in each case.

the Bader analysis[60−62] and the Mulliken analysis,[63−65] to determine the atomic charge (i.e., electron-donating capacity) of the involved surface Fe atoms on each facet for the CO activation. Parts b and c of Figure 4 show the CO activation barrier (E_a) as a function of the Bader charge (q_B) or Mulliken charge (q_M) of the involved surface Fe atoms for the CO activation, respectively. We find that both the atomic charges follow nearly linear relations with the CO activation barrier, suggesting the atomic charge as a dominant factor for the CO activation. To understand the linear relations, we further analyzed the net charges of the C−O atoms and the charge donations of the involved surface Fe atoms in the TSs. It is shown in SI Figure S9 that the charge of the involved surface Fe atoms mainly donates electrons to the TS and thus to affect the stability of the TS. Therefore, the atomic charge of the involved surface Fe atoms for the CO activation is suggested as a dominant factor to describe the CO activation on different χ-Fe_5C_2 catalyst surfaces.

It is also interesting to note from Figure 4b,c as well as SI Figure S6 that for the nine χ-Fe_5C_2 surfaces, different local environment of the involved surface Fe atoms for the CO activation gives rise to significantly different atomic charge, i.e., a different capability to donate electrons for the CO activation. Apparently, the less positively charged the involved surface Fe atoms, the easier the CO activation. To test this idea, the commonly employed K promoter,[14,41,42] being an electronic promoter to donate electrons to the catalyst surface metal atoms, is employed to make the involved surface Fe atoms much less positively charged and thus promote the CO activation. As expected, the CO activation barrier decreases on the three representative K-promoted χ-Fe_5C_2 surfaces compared to their perfect surface, which suggests that the charge of

the involved surface Fe atoms is still the dominant factor for the CO activation on the promoted χ-Fe_5C_2 surfaces.

Furthermore, other representative cases involving the nonstoichiometric terminations which are theoretically evidenced to be stable based on ab initio atomistic thermodynamics[38] and carbon vacancy formed by the Mars–van Krevelen mechanism[37,39,40] are studied to explore the universality of the above linear relations, and the results are shown in Figure 4b,c as well as SI Figure S10. It is found that these typical cases nearly follow the linear relations. This demonstrates the universality of the linear relations. In other words, the atomic charge of the involved surface Fe atoms for the CO activation is evidenced as a dominant factor for the CO activation on the χ-Fe_5C_2 catalyst.

On the basis of the above analyses, our results clearly demonstrate the spatially resolved atomic charge of the involved surface Fe atoms for the CO activation as a better descriptor than the d-band center over the χ-Fe_5C_2 catalyst. The weak correlation of the barrier with the d-band center could arise from another important factor, i.e., the distribution of the d-band,[66,67] not being considered. We expect that the charge could be a generally dominant factor to determine reactant activation on nonuniform catalysts such as metal carbides, nitrides, and sulfides.

To the best of our knowledge, we found for the first time that the difference in the CO activation activities of different χ-Fe_5C_2 catalyst surfaces mainly originates from the difference in the atomic charge of the involved surface Fe atoms for the CO activation. In other words, if the C atoms of the χ-Fe_5C_2 catalyst surfaces withdraw fewer electrons from the involved surface Fe atoms for the CO activation, the involved surface Fe atoms have the stronger ability to activate CO. On the basis of the above analysis, we propose the linear correlation between the CO activation barrier and the charge of the involved surface Fe atoms for CO activation as a unifying concept for understanding the CO activation over the χ-Fe_5C_2 catalyst. Considering the fact that selectivity is another important parameter for the FTS and a direct relationship between the χ-Fe_5C_2 crystal facet and FTS selectivity is still unclear, we will investigate this relationship in our future work.

In summary, we have theoretically revealed the underlying nature of unique CO activation behaviors over the χ-Fe_5C_2 Fischer–Tropsch catalyst. The BEP relation is nearly valid for this system, which is explained and rationalized by the stability of the product. A local site property, i.e., the atomic charge of the involved surface Fe atoms for the CO activation is discriminated as a dominant factor to describe the CO activation on different χ-Fe_5C_2 catalyst surfaces. Specifically, a linear relationship exists between the atomic charge and the CO activation barrier, which is applicable to more complex cases involving the K promoter, nonstoichiometric termination, and/or carbon vacancy. These findings may shed new light on the rational design of χ-Fe_5C_2 FTS catalyst, and the methodology developed here could be applicable for quantifying the structure sensitivity of other (iron) carbides catalysts.

■ ASSOCIATED CONTENT

Supporting Information

The Supporting Information is available free of charge on the ACS Publications website at DOI: 10.1021/acscatal.7b04370.

Computational details (PDF)

■ AUTHOR INFORMATION

Corresponding Authors

*E-mail: chen@nt.ntnu.no.

*E-mail: xzduan@ecust.edu.cn

ORCID

Xuezhi Duan: 0000-0002-5843-5950

Wei Liu: 0000-0003-3016-7381

Yefei Li: 0000-0003-4433-7433

Anders Holmen: 0000-0001-7967-9711

De Chen: 0000-0002-5609-5825

Author Contributions

[⊥](B.C., D.W.) These authors contributed equally.

Notes

The authors declare no competing financial interest.

■ ACKNOWLEDGMENTS

This work was supported by the Natural Science Foundation of China (21776077), Shanghai NSF (17ZR1407300 and 17ZR1407500), the Program for Professor of Special Appointment (Eastern Scholar) at Shanghai Institutions of Higher Learning, the Shanghai Rising-Star Program (17QA1401200), Open Project of SKLOCE (SKL-Che-15C03), Fundamental Research Funds for the Central Universities (22201718003), and the 111 Project of the Ministry of Education of China (B08021).

■ REFERENCES

(1) Torres Galvis, H. M.; de Jong, K. P. Catalysts for Production of Lower Olefins from Synthesis Gas: A Review. *ACS Catal.* **2013**, *3*, 2130–2149.

(2) Wang, D.; Chen, B. X.; Duan, X. Z.; Chen, D.; Zhou, X. G. Iron-Based Fischer–Tropsch Synthesis of Lower Olefins: The Nature of χ-Fe_5C_2 Catalyst and Why and How to Introduce Promoters. *J. Energy Chem.* **2016**, *25*, 911–916.

(3) Zhang, Q. H.; Kang, J. C.; Wang, Y. Development of Novel Catalysts for Fischer–Tropsch Synthesis: Tuning the Product Selectivity. *ChemCatChem* **2010**, *2*, 1030–1058.

(4) Davis, B. H. Fischer–Tropsch Synthesis: Relationship between Iron Catalyst Composition and Process Variables. *Catal. Today* **2003**, *84*, 83–98.

(5) Torres Galvis, H. M.; Bitter, J. H.; Khare, C. B.; Ruitenbeek, M.; Dugulan, A. I.; de Jong, K. P. Supported Iron Nanoparticles as Catalysts for Sustainable Production of Lower Olefins. *Science* **2012**, *335*, 835–838.

(6) de Smit, E.; Weckhuysen, B. M. The Renaissance of Iron-based Fischer–Tropsch Synthesis: on the Multifaceted Catalyst Deactivation Behavior. *Chem. Soc. Rev.* **2008**, *37*, 2758–2781.

(7) Zhai, P.; Xu, C.; Gao, R.; Liu, X.; Li, M. Z.; Li, W. Z.; Fu, X. P.; Jia, C. J.; Xie, J. L.; Zhao, M.; Wang, X. P.; Li, Y. W.; Zhang, Q. W.; Wen, X. D.; Ma, D. Highly Tunable Selectivity for Syngas-Derived Alkenes over Zinc and Sodium-Modulated Fe_5C_2 Catalyst. *Angew. Chem., Int. Ed.* **2016**, *55*, 9902–9907.

(8) Pham, T. H.; Qi, Y. Y.; Yang, J.; Duan, X. Z.; Qian, G.; Zhou, X. G.; Chen, D.; Yuan, W. K. Insights into Hägg Iron-Carbide-Catalyzed Fischer–Tropsch Synthesis: Suppression of CH_4 Formation and Enhancement of C-C Coupling on χ-Fe_5C_2 (510). *ACS Catal.* **2015**, *5*, 2203–2208.

(9) Torres Galvis, H. M.; Bitter, J. H.; Davidian, T.; Ruitenbeek, M.; Dugulan, A. I.; de Jong, K. P. Iron Particle Size Effects for Direct Production of Lower Olefins from Synthesis Gas. *J. Am. Chem. Soc.* **2012**, *134*, 16207–16215.

(10) Barkhuizen, D.; Mabaso, I.; Viljoen, E.; Welker, C.; Claeys, M.; van Steen, E.; Fletcher, J. C. Q. Experimental Approaches to the Preparation of Supported Metal Nanoparticles. *Pure Appl. Chem.* **2006**, *78*, 1759–1769.

(11) de Smit, E.; Cinquini, F.; Beale, A. M.; Safonova, O. V.; van Beek, W.; Sautet, P.; Weckhuysen, B. M. Stability and Reactivity of ϵ-χ-θ Iron Carbide Catalyst Phases in Fischer–Tropsch Synthesis: Controlling μ_C. *J. Am. Chem. Soc.* **2010**, *132*, 14928–14941.
(12) Liu, X.; Zhang, C. H.; Li, Y. W.; Niemantsverdriet, J. W.; Wagner, J. B.; Hansen, T. W. Environmental Transmission Electron Microscopy (ETEM) Studies of Single Iron Nanoparticle Carburization in Synthesis Gas. *ACS Catal.* **2017**, *7*, 4867–4875.
(13) Yang, C.; Zhao, H. B.; Hou, Y. L.; Ma, D. Fe_5C_2 Nanoparticles: A Facile Bromide-Induced Synthesis and as an Active Phase for Fischer–Tropsch Synthesis. *J. Am. Chem. Soc.* **2012**, *134*, 15814–15821.
(14) Park, J. C.; Yeo, S. C.; Chun, D. H.; Lim, J. T.; Yang, J. I.; Lee, H. T.; Hong, S.; Lee, H. M.; Kim, C. S.; Jung, H. Highly Activated K-doped Iron Carbide Nanocatalysts Designed by Computational Simulation for Fischer–Tropsch Synthesis. *J. Mater. Chem. A* **2014**, *2*, 14371–14379.
(15) Gu, B.; He, S.; Zhou, W.; Kang, J. C.; Cheng, K.; Zhang, Q. H.; Wang, Y. Polyaniline-Supported Iron Catalyst for Selective Synthesis of Lower Olefins from Syngas. *J. Energy Chem.* **2017**, *26*, 608–615.
(16) Jiang, F.; Liu, B.; Li, W. P.; Zhang, M.; Li, Z. J.; Liu, X. H. Two-Dimensional Graphene-Directed Formation of Cylindrical Iron Carbide Nanocapsules for Fischer–Tropsch Synthesis. *Catal. Sci. Technol.* **2017**, *7*, 4609–4621.
(17) An, B.; Cheng, K.; Wang, C.; Wang, Y.; Lin, W. B. Pyrolysis of Metal-Organic Frameworks to Fe_3O_4@Fe_5C_2 Core-Shell Nanoparticles for Fischer–Tropsch Synthesis. *ACS Catal.* **2016**, *6*, 3610–3618.
(18) Cheng, J.; Hu, P.; Ellis, P.; French, S.; Kelly, G.; Lok, C. M. Density Functional Theory Study of Iron and Cobalt Carbides for Fischer–Tropsch Synthesis. *J. Phys. Chem. C* **2010**, *114*, 1085–1093.
(19) O'Brien, R. J.; Xu, L.; Spicer, R. L.; Davis, B. H. Activation Study of Precipitated Iron Fischer–Tropsch Catalysts. *Energy Fuels* **1996**, *10*, 921–926.
(20) Yang, Z. Y.; Zhao, T. S.; Huang, X. X.; Chu, X.; Tang, T. Y.; Ju, Y. M.; Wang, Q.; Hou, Y. L.; Gao, S. Modulating the Phases of Iron Carbide Nanoparticles: From a Perspective of Interfering with the Carbon Penetration of Fe@Fe_3O_4 by Selectively Adsorbed Halide Ions. *Chem. Sci.* **2017**, *8*, 473–481.
(21) Yao, S. Y.; Yang, C.; Zhao, H. B.; Li, S. W.; Lin, L. L.; Wen, W.; Liu, J. X.; Hu, G.; Li, W. X.; Hou, Y. L.; Ma, D. Reconstruction of the Wet Chemical Synthesis Process: The Case of Fe_5C_2 Nanoparticles. *J. Phys. Chem. C* **2017**, *121*, 5154–5160.
(22) Yang, C.; Zhao, B.; Gao, R.; Yao, S. Y.; Zhai, P.; Li, S. W.; Yu, J.; Hou, Y. L.; Ma, D. Construction of Synergistic Fe_5C_2/Co Heterostructured Nanoparticles as an Enhanced Low Temperature Fischer–Tropsch Synthesis Catalyst. *ACS Catal.* **2017**, *7*, 5661–5667.
(23) Liu, Z. P.; Hu, P. General Rules for Predicting Where a Catalytic Reaction Should Occur on Metal Surfaces: A Density Functional Theory Study of C-H and C-O Bond Breaking/Making on Flat, Stepped, and Kinked Metal Surfaces. *J. Am. Chem. Soc.* **2003**, *125*, 1958–1967.
(24) Shetty, S.; Jansen, A. P. J.; van Santen, R. A. Direct versus Hydrogen-Assisted CO Dissociation. *J. Am. Chem. Soc.* **2009**, *131*, 12874–12875.
(25) Ge, Q.; Neurock, M. Adsorption and Activation of CO over Flat and Stepped Co Surfaces: A First Principles Analysis. *J. Phys. Chem. B* **2006**, *110*, 15368–15380.
(26) Yang, J.; Qi, Y. Y.; Zhu, J.; Zhu, Y. A.; Chen, D.; Holmen, A. Reaction Mechanism of CO Activation and Methane Formation on Co Fischer–Tropsch Catalyst: A Combined DFT, Transient, and Steady-State Kinetic Modeling. *J. Catal.* **2013**, *308*, 37–49.
(27) Nørskov, J. K.; Bligaard, T.; Rossmeisl, J.; Christensen, C. H. Towards the Computational Design of Solid Catalysts. *Nat. Chem.* **2009**, *1*, 37–46.
(28) Michaelides, A.; Liu, Z. P.; Zhang, C. J.; Alavi, A.; King, D. A.; Hu, P. Identification of General Linear Relationships between Activation Energies and Enthalpy Changes for Dissociation Reactions at Surfaces. *J. Am. Chem. Soc.* **2003**, *125*, 3704–3705.
(29) Cheng, J.; Hu, P.; Ellis, P.; French, S.; Kelly, G.; Lok, C. M. Brønsted-Evans-Polanyi Relation of Multistep Reactions and Volcano Curve in Heterogeneous Catalysis. *J. Phys. Chem. C* **2008**, *112*, 1308–1311.
(30) Van Santen, R. A. Complementary Structure Sensitive and Insensitive Catalytic Relationships. *Acc. Chem. Res.* **2009**, *42*, 57–66.
(31) Mavrikakis, M.; Hammer, B.; Nørskov, J. K. Effect of Strain on the Reactivity of Metal Surfaces. *Phys. Rev. Lett.* **1998**, *81*, 2819–2822.
(32) Liu, J. X.; Su, H. Y.; Sun, D. P.; Zhang, B. Y.; Li, W. X. Crystallographic Dependence of CO Activation on Cobalt Catalysts: HCP versus FCC. *J. Am. Chem. Soc.* **2013**, *135*, 16284–16287.
(33) Liu, J. X.; Li, W. X. Theoretical Study of Crystal Phase Effect in Heterogeneous Catalysis. *Wiley Interdiscip. Rev.: Comput. Mol. Sci.* **2016**, *6*, 571–583.
(34) Pham, T. H.; Duan, X. Z.; Qian, G.; Zhou, X. G.; Chen, D. CO Activation Pathways of Fischer–Tropsch Synthesis on χ-Fe_5C_2 (510): Direct versus Hydrogen-Assisted CO Dissociation. *J. Phys. Chem. C* **2014**, *118*, 10170–10176.
(35) Huo, C. F.; Li, Y. W.; Wang, J.; Jiao, H. J. Insight into CH_4 Formation in Iron-Catalyzed Fischer–Tropsch Synthesis. *J. Am. Chem. Soc.* **2009**, *131*, 14713–14721.
(36) Cao, D. B.; Li, Y. W.; Wang, J.; Jiao, H. J. Chain Growth Mechanism of Fischer–Tropsch Synthesis on Fe_5C_2(001). *J. Mol. Catal. A: Chem.* **2011**, *346*, 55–69.
(37) Gracia, J. M.; Prinsloo, F. F.; Niemantsverdriet, J. W. Mars-van Krevelen-like Mechanism of CO Hydrogenation on an Iron Carbide Surface. *Catal. Lett.* **2009**, *133*, 257–261.
(38) Zhao, S.; Liu, X. W.; Huo, C. F.; Li, Y. W.; Wang, J. G.; Jiao, H. J. Determining Surface Structure and Stability of ϵ-Fe_2C, χ-Fe_5C_2, θ-Fe_3C and Fe_4C Phases under Carburization Environment from Combined DFT and Atomistic Thermodynamic Studies. *Catal., Struct. React.* **2015**, *1*, 44–60.
(39) Ozbek, M. O.; Niemantsverdriet, J. W. Elementary Reactions of CO and H_2 on C-terminated χ-Fe_5C_2(001) Surfaces. *J. Catal.* **2014**, *317*, 158–166.
(40) Petersen, M. A.; van Rensburg, W. J. CO Dissociation at Vacancy Sites on Hägg Iron Carbide: Direct Versus Hydrogen-Assisted Routes Investigated with DFT. *Top. Catal.* **2015**, *58*, 665–674.
(41) Petersen, M. A.; Cariem, M. J.; Claeys, M.; van Steen, E. A DFT Perspective of Potassium Promotion of χ-Fe_5C_2(100). *Appl. Catal., A* **2015**, *496*, 64–72.
(42) Zhao, S.; Liu, X. W.; Huo, C. F.; Li, Y. W.; Wang, J. G.; Jiao, H. J. The Role of Potassium Promoter in Surface Carbon Hydrogenation on Hägg Carbide Surfaces. *Appl. Catal., A* **2015**, *493*, 68–76.
(43) Sorescu, D. C. Plane-Wave DFT Investigations of the Adsorption, Diffusion, and Activation of CO on Kinked Fe(710) and Fe(310) Surfaces. *J. Phys. Chem. C* **2008**, *112*, 10472–10489.
(44) Gong, X. Q.; Raval, R.; Hu, P. CO Dissociation and O Removal on Co(0001): A Density Functional Theory Study. *Surf. Sci.* **2004**, *562*, 247–256.
(45) Qi, Y. Y.; Yang, J.; Chen, D.; Holmen, A. Recent Progresses in Understanding of Co-Based Fischer–Tropsch Catalysis by Means of Transient Kinetic Studies and Theoretical Analysis. *Catal. Lett.* **2015**, *145*, 145–161.
(46) Petersen, M. A.; van den Berg, J. A.; Ciobîca, I. M.; van Helden, P. Revisiting CO Activation on Co Catalysts: Impact of Step and Kink Sites from DFT. *ACS Catal.* **2017**, *7*, 1984–1992.
(47) Retief, J. J. Powder Diffraction Data and Rietveld Refinement of Hägg-Carbide, χ-Fe_5C_2. *Powder Diffr.* **1999**, *14*, 130–132.
(48) Medford, A. J.; Vojvodic, A.; Hummelshøj, J. S.; Voss, J.; Abild-Pedersen, F.; Studt, F.; Bligaard, T.; Nilsson, A.; Nørskov, J. K. From the Sabatier Principle to a Predictive Theory of Transition-Metal Heterogeneous Catalysis. *J. Catal.* **2015**, *328*, 36–42.
(49) Montemore, M. M.; Medlin, J. W. Scaling Relations between Adsorption Energies for Computational Screening and Design of Catalysts. *Catal. Sci. Technol.* **2014**, *4*, 3748–3761.
(50) Bronsted, J. N. Acid and Basic Catalysis. *Chem. Rev.* **1928**, *5*, 231–338.

(51) Bell, R. P. The Theory of Reactions Involving Proton Transfers. *Proc. R. Soc. London, Ser. A* **1936**, *154*, 414−429.
(52) Evans, M. G.; Polanyi, M. Inertia and Driving Force of Chemical Reactions. *Trans. Faraday Soc.* **1938**, *34*, 11−24.
(53) Hammond, G. S. A Correlation of Reaction Rates. *J. Am. Chem. Soc.* **1955**, *77*, 334−338.
(54) Pallassana, V.; Neurock, M. Electronic Factors Governing Ethylene Hydrogenation and Dehydrogenation Activity of Pseudomorphic Pd_{ML}/Re(0001), Pd_{ML}/Ru(0001), Pd(111), and Pd_{ML}/Au(111) Surfaces. *J. Catal.* **2000**, *191*, 301−317.
(55) Hammer, B.; Nørskov, J. K. Electronic Factors Determining the Reactivity of Metal Surfaces. *Surf. Sci.* **1995**, *343*, 211−220.
(56) Hammer, B.; Nørskov, J. K. Theoretical Surface Science and Catalysis - Calculations and Concepts. *Adv. Catal.* **2000**, *45*, 71−129.
(57) Montemore, M. M.; Medlin, J. W. Site-Specific Scaling Relations for Hydrocarbon Adsorption on Hexagonal Transition Metal Surfaces. *J. Phys. Chem. C* **2013**, *117*, 20078−20088.
(58) Hyman, M. P.; Medlin, J. W. Effects of Electronic Structure Modifications on the Adsorption of Oxygen Reduction Reaction Intermediates on Model Pt(111)-Alloy Surfaces. *J. Phys. Chem. C* **2007**, *111*, 17052−17060.
(59) Xie, J. X.; Yang, J.; Dugulan, A. I.; Holmen, A.; Chen, D.; de Jong, K. P.; Louwerse, M. J. Size and Promoter Effects in Supported Iron Fischer−Tropsch Catalysts: Insights from Experiment and Theory. *ACS Catal.* **2016**, *6*, 3147−3157.
(60) Bader, R. F. W. *Atoms in Molecules: A Quantum Theory*; Clarendon Press: Oxford, UK, 1994.
(61) Henkelman, G.; Arnaldsson, A.; Jónsson, H. A Fast and Robust Algorithm for Bader Decomposition of Charge Density. *Comput. Mater. Sci.* **2006**, *36*, 354−360.
(62) Sanville, E.; Kenny, S. D.; Smith, R.; Henkelman, G. Improved Grid-Based Algorithm for Bader Charge Allocation. *J. Comput. Chem.* **2007**, *28*, 899−908.
(63) Mulliken, R. S. Electronic Population Analysis on LCAO-MO Molecular Wave Functions. I. *J. Chem. Phys.* **1955**, *23*, 1833−1840.
(64) Mulliken, R. S. Electronic Population Analysis on LCAO-MO Molecular Wave Functions. II. Overlap Populations, Bond Orders, and Covalent Bond Energies. *J. Chem. Phys.* **1955**, *23*, 1841−1846.
(65) Mulliken, R. S. Electronic Population Analysis on LCAO-MO Molecular Wave Functions. IV. Bonding and Antibonding in LCAO and Valence-Bond Theories. *J. Chem. Phys.* **1955**, *23*, 2343−2346.
(66) Huang, B.; Xiao, L.; Lu, J. T.; Zhuang, L. Spatially Resolved Quantification of the Surface Reactivity of Solid Catalysts. *Angew. Chem., Int. Ed.* **2016**, *55*, 6239−6243.
(67) Vojvodic, A.; Nørskov, J. K.; Abild-Pedersen, F. Electronic Structure Effects in Transition Metal Surface Chemistry. *Top. Catal.* **2014**, *57*, 25−32.